This is a preprint, the final version is subject to change, of the American Mineralogist (MSA)
Cite as Authors (Year) Title. American Mineralogist, in press.
DOI: https://doi.org/10.2138/am-2020-7202

Revision 2

Deconvolution of the composition of fine-grained pyrite in sedimentary matrix by regression of time-resolved LA-ICP-MS data

Aleksandr S. Stepanov[a, b], Leonid V. Danyushevsky[b], Ross R. Large[b], Indrani Mukherjee[b], Irina A. Zhukova[a, b]

[a]School of Earth Resources, Collaborative Innovation Center for Exploration of Strategic Mineral Resources, China University of Geosciences, Wuhan 430074, China

[b]CODES Centre for Ore Deposit and Earth Sciences, Private Bag 126, University of Tasmania, Hobart, TAS 7001, Australia

Abstract

Pyrite is a common mineral in sedimentary rocks and is the major host for many chalcophile trace elements utilized as important tracers of the evolution of the ancient hydrosphere. Measurement of trace element composition of pyrite in sedimentary rocks is challenging due to fine grain size and intergrowth with silicate matrix and other sulfide minerals. In this contribution, we describe a method for calculation of trace element composition of sedimentary pyrite from time-resolved LA-ICP-MS data. The method involves analysis of both pyrite and pyrite-free sediment matrix, segmentation of LA-ICP-MS spectra, normalization to total, regression analysis of dependencies between the elements and calculation of normalized composition of the mineral. Sulfur is chosen as an

explanatory variable, relative to which all regressions are calculated. The S content value used for calculation of element concentrations from the regressions is calculated from the total, eliminating the need for independent constraints. The algorithm allows efficient measurement of concentrations of multiple chalcophile trace elements in pyrite in a wide range of samples, including quantification of detection limits and uncertainties while excluding operator bias. The data suggest that the main sources of uncertainties on pyrite composition are sample heterogeneity and counting statistics for elements of low abundance. The analysis of regression data of time-resolved LA-ICP-MS measurements could provide new insights to the geochemistry of the sedimentary rocks and minerals. It allows quantification of ratios of elements that do not have reference material available (such as Hg) and provides estimates on content of non-sulfidic Fe in the silicate matrix. Regression analysis of the mixed LA-ICP-MS signal could be a powerful technique for deconvolution of phase compositions in complex multicomponent samples.

Highlights:

- Sedimentary pyrite is an important host of many trace elements
- LA-ICP-MS analysis of sedimentary pyrite results in variable, mixed data
- Pyrite composition is calculated from the mixed data using an algorithm based on linear regression
- The algorithm involves segmentation of the time-resolved signal, normalization to total, calculation of the regression equations and estimation of explanatory variable normalizing to total

- Regression analysis of time-resolved mixed LA-ICP-MS data is a powerful technique for analysis of complex substances

This is a preprint, the final version is subject to change, of the American Mineralogist (MSA)
Cite as Authors (Year) Title. American Mineralogist, in press.
DOI: https://doi.org/10.2138/am-2020-7202

Introduction

Pyrite is a common mineral in sedimentary rocks and can host a wide range of trace elements (e. g., Abraitis et al. 2004; Gregory et al. 2015). Trace element compositions of pyrite have been applied to various geochemical problems ranging from tracing chemistry of paleo oceans, nutrient availability and evolution of the atmosphere and biosphere (Huerta-Diaz and Morse 1990; Large et al. 2014, 2015b, 2015a; Gregory et al. 2015; Zhou et al. 2017; Rickard et al. 2017) to release of economically-important elements during metamorphism (Pitcairn et al. 2010; Large et al. 2011; Tomkins 2013; Goldfarb and Groves 2015). The content of pyrite and its trace element composition in sedimentary rocks can be measured by selective digestions by acids (Huerta-Diaz and Morse 1990; Raiswell et al. 1994); however, such methods yield average compositions of pyrite and cannot resolve different generations of the mineral. The challenges for *in situ* analysis of pyrite in sedimentary rocks include fine grain size, low concentration levels of many key elements, abundant inclusions of matrix minerals and intergrowth with other sulfides (Fig. 1).

LA-ICP-MS is a powerful analytical technique commonly applied for analysis of pyrite (e.g. Large et al. 2009). Typical analyses are performed by a round laser spot with diameter 20-30 μm but in many sedimentary rocks the size of pyrite is smaller than lateral spatial resolution of the laser (Fig. 1). Analysis could be performed with smaller spot sizes, however, this is rarely practical due to decrease of signal and increase of downhole elemental fractionation (Gilbert et al. 2014a).

Analysis of sedimentary pyrite by LA-ICP-MS results in the acquisition of complex mixed data with variable contributions from phases other than pyrite (Fig. 2). There are two principal methods of recalculation of the mixed compositional data: subtraction and regression (Stepanov et al. 2012). When applied to pyrite, both methods involve analysis of matrix of the rock with minimal pyrite content and mixtures of the pyrite and matrix (Large et al. 2014). For the subtraction method, the integration interval with high pyrite content is selected from the transient signal of the mixed analysis. The weight fractions of the pyrite in the mixture is then calculated from pyrite stoichiometric Fe content, followed by the subtraction of the matrix component from the mixed analysis. This method has a number of limitations such as an assumption of a constant composition of the matrix across the sample, subjective selection of the integration interval and the complexity of propagation of the uncertainties into the final compositions.

Regression analysis is a statistical method for quantification of the dependencies between variables, which previously has been applied to deconvolution of mixed LA-ICP-MS analyzes of fine grains of accessory minerals in glasses for experimental work on mineral/melt partitioning of trace elements (Rubatto and Hermann 2007; Stepanov et al. 2012; Taylor et al. 2015). In this contribution we present new developments in the application of regression analysis to measurement of pyrite trace element composition in black shales by LA-ICP-MS, which overcome the major problems of the subtraction method. We describe the algorithm which is capable of generating self-consistent compositions of pyrite in complex matrixes and is able to estimate uncertainty of the data and detection limits without assumptions on the composition of the sulfide or its grain

size. We also discuss the application of the regression approach to analysis of some geochemical features of the sedimentary rocks.

Analytical technique

The samples of black shales were cut by diamond saw and mounted into 25 mm round epoxy blocks and polished. Samples were analyzed for trace elements at CODES Analytical Laboratories, University of Tasmania. A RESOlution 193 nm excimer laser ablation system coupled with an Agilent 7700 ICP-MS was used for all analyses. The instrument is equipped with a Laurin Technic S155 ablation cell capable of housing sample holders with up to 20 epoxy blocks. Samples were ablated in an atmosphere of pure He flowing at a rate of 0.35 L/min. Helium carrier gas was mixed with Ar make-up gas flowing at 1.05 L/min outside the ablation chamber. The ICP-MS was optimized to maximize sensitivity on mid to high-masses (in the range 80–240 amu) and minimize production of molecular oxide species ($^{232}Th^{16}O^{+}/^{232}Th^{+}$) at < 0.2%. During each analysis a background signal was recorded for 30 seconds, after which the laser was turned on and the sample was ablated for 30-60 seconds. The laser repetition rate was 5 Hz and the laser fluence was set to 2.7 J cm^{-2} for sulfides and SDGL2b2 reference material (Danyushevsky et al., 2011) while fluence 3 J cm^{-2} was used for GSD-1g glass. Moisture and air absorbed to the sample could cause significant deleterious effect on LA-ICP-MS analyses by increasing drift and interferences (Thompson et al. 2018). All samples analyzed in this study were degassed under vacuum for at least 12 hours prior to analysis.

During analytical sessions two varieties of spot analyses were collected on the sample. One type was analysis of the sedimentary matrix which contained minimal

115 amounts of pyrite and is referred to hereafter as matrix analyses. Another type was
116 analysis of pyrite grains of different textural types referred to hereafter as pyrite analyses.
117 The laser beam size used for the ablation was between 10 and 50 μm in diameter;
118 however, most pyrite analyses were performed with 20 to 30 μm beam, depending on the
119 grain size. The matrix analyses were acquired with either the same beam size as the pyrite
120 or with a 50 μm beam, in order to improve the detection limits for elements at low
121 abundance, providing pyrite-free areas in the matrix were large enough.

122 The ICP-MS method used in this study comprised 42 masses (Table 1). The major
123 elements were measured to allow quantification of concentrations by normalization to a
124 total. Tantalum and Gd were measured to assess interferences on Au. The dwell times
125 ranged from 5 ms for major elements to 50 ms for low abundance chalcophile elements
126 such as Au, Se and Te (Table 1).

127 An in-house pyrite reference material (PPP-1, Gilbert et al. 2014b) was analyzed
128 with the same spot size as unknown pyrite for sulfur calibration in order to account for
129 downhole fractionation during ablation of pyrite (Gilbert et al. 2014a). Reference
130 material GSD-1g (Guillong et al. 2005) was used for calibration of lithophile elements
131 and an in-house reference material STDGL2b2 (Danyushevsky et al. 2011) was used for
132 calibration of chalcophile and siderophile elements (see Table 1 for details). Each batch
133 of analyses included two sets of calibration reference materials at the beginning and end
134 of the batch, and 15 to 30 analyses on the samples. Each set of reference materials
135 included 6 analyses (each reference material was analyzed twice). On each sample, 5-7
136 analyses were performed on the “matrix” and 10-15 analyses on pyrite.

This is a preprint, the final version is subject to change, of the American Mineralogist (MSA)
Cite as Authors (Year) Title. American Mineralogist, in press.
DOI: https://doi.org/10.2138/am-2020-7202

Algorithm

The derivation of pyrite composition from the mixed signal involves segmentation of the signal, primary standardization, recalculation to the total, calculation of the linear regression, estimation of the internal standard value for regression, calculation of the final values, estimation of uncertainties from regressions and filtering of values below the detection limits. Each step is described in detail below, followed by a summary of the data reduction procedure.

Segmentation of the signal

Ablation of a sulfide grain in the matrix results in highly variable time-resolved spectra (Fig. 2). The time-resolved LA signal was divided into five segments of identical duration (Fig. 2a). The number of segments has been chosen to obtain a sufficient number of points for regression analysis, and also to ensure that the number of data points in each segment is sufficient to yield a meaningful average signal for elements of low abundance. The segmentation of the signal was performed using an automated script which sets the same integration interval for all reference materials and unknowns. The effect of downhole fractionation on analytical results was therefore minimized by quantifying every segment using the identical time interval on reference materials.

Primary quantification and normalization of the analyses

Quantification of LA-ICP-MS data requires knowledge of the concentration of at least one element – the internal standard (Longerich et al., 1996). However, by the very nature of analysis of a heterogeneous aggregate of grains of pyrite in matrix, concentrations of all elements vary both between analyses and during ablation. Therefore, internal standardization was performed in two stages. At the first stage when preliminary

160 concentrations were calculated, stoichiometric content of Fe in pyrite was used as the
161 internal standard value. Preliminary concentrations were calculated following the
162 protocol established by Longerich et al. (1996):

163 $$C_{El}^{Sam} = \frac{R_{El}^{Sam}}{S} \quad (1)$$

164 Where C_{El}^{Sam} is the concentration of element El in the sample, R_{El}^{Sam} is count rate of the
165 element and S in the normalized sensitivity calculated as:

166 $$S = \frac{R_{El}^{Cal}}{C_{El}^{Cal}} \left(\frac{R_{Fe}^{Sam}}{R_{Fe}^{Cal}} * \frac{C_{Fe}^{Cal}}{C_{Fe}^{Sam}}\right) \quad (2)$$

167 Where C_{El}^{Cal} is the concentration of the element in the reference material used for the
168 calibration of the element; R_{El}^{Cal} is measured count rate of the element in the reference
169 material; R_{Fe}^{Sam} is count rate of Fe measured on sample and R_{Fe}^{Cal} measured on the
170 calibration standard; C_{Fe}^{Sam} is the concentration of Fe in the sample, which was set to the
171 stoichiometric Fe content in pyrite; and C_{Fe}^{Cal} is content of Fe in the reference material
172 used for calibration of the element El. The instrumental drift and mass bias were
173 constrained at this stage by using a linear fit to standards for each analytical batch.

174 The second stage quantification was performed by normalising the sum of all
175 elements to 1,000,000 ppm (Leach and Hieftje 2000; Liu et al. 2010). In the case of
176 mixed pyrite-sediment data, we assume that lithophile elements (Na, Mg, Al, Si, K, Ca,
177 Ti, V, Cr, Mn, Rb, Sr, Zr, Ba, Gd, Hf, Ta, Th and U) are present as oxides in silicate
178 matrix and inclusions and other elements (Co, Ni, Cu, Zn, As, Se, Mo, Ag, Cd, Sn, Sb, Te,
179 W, Pt, Au, Tl, Pb, Bi) occur as sulfides. Therefore, the second stage normalization was
180 performed using the coefficient defined as:

$$c = 1{,}000{,}000/(\sum_{all} C_{El} + 16 * \sum_{lith} C_{El} N_{El}^{O} / M_{El}) \quad (3)$$

Where the first member $\sum_{all} C_{El}$ is sum of the concentrations of all measured elements and the second member $16 * \sum_{lith} C_{El} * N_{El}^{O} / M_{El}$ is mass of oxygen in oxides of lithophile elements, where C_{El} is the concentration of lithophile element, M_{El} is atomic mass of the element and N_{El}^{O} is number of oxygen atoms per atom of metal. All Fe is assumed to reside in sulfide at this stage of calculations.

Regression analysis of the data

After the normalization of the data, the segmented analyses commonly show strong correlations between chalcophile elements residing in pyrite (Fig. 3). For regression analysis, one needs to choose an explanatory (independent) variable. For pyrite, both S and Fe could be used as explanatory variables; however, S was chosen as the more versatile component present in all sulfides. Linear minimal squares regression implemented in Excel was used for quantification of the regression dependencies (see Supplementary table for an example of calculation).

The relation between an element and sulfur is described by the regression equations:

$$C_{El} = C_S A_{El} + B_{El} \quad (4)$$

Where C_{El} is the concentration of an element and C_S is sulfur content in the mineral. A_{El} and B_{El} are the slope and the intercept of the regression.

There are several options for choosing the data for regression. Our default option is a regression through segmented pyrite analyses and segmented matrix analyses (Fig 3), which is referred to below as "pyrite+matrix". An alternative option is calculation of the regression from five points of the segmented pyrite analysis alone, which is referred as "pyrite only" hereafter. Since there are more analyses of the matrix in the dataset, the low-S end of the "pyrite+matrix" regression is well constrained. Segments rich in pyrite mainly define the slope of the regression line.

However, there are instances when a regression based on pyrite and matrix analyzes could give erroneous results:

- The distribution of an element is highly variable in the matrix (Fig. 4a). In this case the regression based on pyrite and matrix data would pass though the average of the matrix data, whereas the local matrix measured in such a case might be better constrained by the regression calculated from "pyrite only".
- Pyrite is mixed with a matrix component which is different from the analyzed matrix (Fig. 4b). This situation also could be resolved by calculating a "pyrite only" regression.
- Significant variation in the proportion of pyrite and matrix during the analysis is necessary for constraining the regression equations. However, in some samples pyrite is ubiquitous, and analysis of "pure" matrix without pyrite is not possible (Figs. 1, 4c). In cases when each segment of the pyrite analysis has a similar composition (i.e., the segments are characterized by a relatively constant proportion of the matrix and pyrite), an unconstrained regression may be obtained, when the slope of an Fe-S regression becomes negative, precluding a meaningful set of regression equations (Fig. 5). Non-robust regressions may also occur when there is a difference in the extent of downhole

fractionation of Fe and S between the reference material and pyrite sample. The set of non-robust regressions could predict meaningless negative concentrations of elements. In such situations pyrite compositions also could be calculated by "pyrite only" regression by forcing the "pyrite only" regression line through origin (Fig. 5).

Calculation of concentrations from regression equations

To calculate the concentration of an element from equation 4, a value for the explanatory variable (sulfur in our case) is required. Such value is analogous to the internal standard value, which is commonly estimated from electron probe micro analyzer (EPMA) data or from mineral stoichiometry (Longerich et al., 1996). The explanatory variable value for the set of regression equations could be obtained from the condition that the sum of the mass concentrations of all elements in the analysis is expected to equal 1,000,000 ppm:

$$\sum C_{El} = 1{,}000{,}000 \quad (5)$$

Summation of regression equations (Eq. 4) for all elements leads to:

$$\sum C_{El} = C_S \sum A + \sum B = 1{,}000{,}000 \quad (6)$$

Where $\sum A$ is sum of the regression slopes for all elements and $\sum B$ is sum of the regression intercepts. This equation could be rearranged for calculation of the value of explanatory variable C_S as:

This is a preprint, the final version is subject to change, of the American Mineralogist (MSA)
Cite as Authors (Year) Title. American Mineralogist, in press.
DOI: https://doi.org/10.2138/am-2020-7202

$$C_S = \frac{1{,}000{,}000 - \sum B}{\sum A} \quad (7)$$

Notably this formula is independent of the data set used for estimation of the regression equations and regression for different elements, based on either "pyrite+ matrix" or "pyrite only", could be used.

Estimation of uncertainties

The regression analysis allows estimation of uncertainties on the calculated parameters, including the slope and intercept and the regression prediction. Uncertainty of prediction could be calculated either as the standard error on the mean or the standard error on the forecast (e. g., Montgomery et al. 2012). The standard error on the forecast estimates uncertainty of the next measurement, whereas the standard error on the mean estimates uncertainty on the average. Since the aim of our calculations is to estimate average composition of the ablated pyrite grains, the standard error on the mean is a more suitable measure of uncertainty.

The uncertainty from the regression was calculated as the standard error on the mean from the well known statistical formulae (http://people.duke.edu/~rnau/mathreg.htm, e.g., Desalvo, 1971):

$$\delta_{EL} = \frac{s}{\sqrt{N}} \sqrt{1 + (C_S - Average(C_S))^2 / Stdev(C_S)^2} \quad (8)$$

Where s is standard error of regression calculated as $\sqrt{(N-1)/(N-2)} * (1-r^2) * Stdev(C_{El})$, N number of measurements, r is regression coefficient, C_S is the concentration of sulfur from Eq. 7, $Average(C_S)$ is the average sulfur of the analyses, C_{El} is the concentration of an element for which regression is

265 calculated and Stdev(C_{El}) is the standard deviation of the concentration of an element in
266 the data set.

267 The regression uncertainties have the lowest values at the average S content and
268 increase away from this value (Fig. 6). In the case of "pyrite+matrix" regression, the
269 average is close to the matrix values, which are more numerous than segmented pyrite
270 analyses. This results in an uncertainty estimate which is defined by the heterogeneity of
271 the matrix (Fig. 6). However, the segmented pyrite analyses should define the regression
272 uncertainty since our aim is calculating the pyrite composition. Therefore, the Eq. 8 was
273 modified to:

274 $$\delta_{EL} = \frac{s}{\sqrt{N}} \sqrt{1 + (C_S - Average(C_S^{Py}))^2 / Stdev(C_S^{Py})^2} \quad (9)$$

275 Where C_S^{Py} is sulfur in "pyrite only" data.

276 Assessing compositional variations of elements for which reference
277 materials are not available

278 Quantification of LA-ICP-MS analyses is based on reference materials with the
279 known concentration of the analyte (Longerich et al., 1996). The requirements for
280 reference materials include homogeneity, sufficiently high concentration, limited amount
281 of isobaric interferences and low uncertainty on the accepted value. Unfortunately, such
282 materials are still not available for a number of elements, one of which is Hg.

283 Mercury is an extremely volatile element and it could diffuse from many
284 compounds especially at high temperature. So far, a glass reference material with
285 homogeneous and known Hg content is not available because Hg is mobile during glass
286 preparation. Hg-bearing minerals also are not suitable as reference materials because the

high volatility of Hg results in increased Hg background hampering analysis of Hg in the unknowns. Additionally, high volatility and high density of Hg results in its accumulation, migration and redeposition in the ablation cell.

Mercury is a chalcophile element and it can occur in significant concentrations in pyrite (Wells and Mullens 1973; Griffin et al. 1991; Abraitis et al. 2004). Some analyses of sedimentary pyrite show strong correlations between count ratio $^{202}Hg/^{57}Fe$ and other chalcophile elements (Fig. 7a, b) which is clear evidence for the concentration of Hg in the sedimentary pyrite. Other samples show negative correlations, suggesting that Hg is hosted by the matrix (Fig. 7c). Considering low variability of Fe content in pyrite, Hg/Fe count-rate ratio can be used for comparison of Hg abundances between samples.

Isotope ^{202}Hg was measured along with other isotopes and after the subtraction of the gas background the signal was corrected for instrumentation drift during each session. Mass bias variation between sessions was corrected by calculating $^{206}Pb/^{57}Fe$ fractionation using background corrected signal ratio measured on STDGL2b2 reference material. The calculated Hg/Fe ratios were corrected for yield by the coefficient used for normalization to total (Eq. 3). Regression equation of the segmented signal relative to S was calculated, and the Hg/Fe ratio was extrapolated to the S content calculated by Eq. 7. The ratios have been multiplied by factor of 1000 for reporting (Fig. 7). The calculated Hg/Fe*1000 ratios could be used for qualitative comparison of samples, indicating which samples have higher and lower contents of Hg.

Estimation of limits of detection

Our calculation of the detection limits in compositions of sedimentary pyrite was based on the approach of Longerich et al. (1996). The detection limits for individual

segmented analyzes were calculated from the noise on the gas blank (laser off) using the following formula:

$$DL_{EL} = i * Stdev(BG_{El}) / S_{El} * \sqrt{1/N^{BG} + 1/N^{SM}} \quad (10)$$

Where DL_{EL} is the limit of detection of the element, i is a coefficient defining the threshold above which the signal is accepted as exceeding noise level (3 in this study), S_{El} is normalized sensitivity as calculated by Eq. 2, $Stdev(BG_{El})$ is the standard deviation of the gas blank, N^{BG} is number of measurement (sweeps) of the gas blank and N^{SM} in number of measurements during the ablation of the sample. Masses with low gas background could have all readings zero in some analyses. In order to alleviate this situation and also to obtain more robust estimates of the noise, the average gas blank standard deviation for all analyses measured on sample mounts was used in Eq. 10.

Data reduction procedure

The algorithm presented was implemented in an in-house Excel spreadsheet. Time-resolved spectra were segmented and then the preliminary concentrations were calculated. The validity of the calibration and background correction was checked by an operator. At the next stage, normalization to a total of 1,000,000 ppm was performed, followed by the generation of regression plots for individual analyses (Fig. 3-5). The matrix analyses were inspected for the presence of pyrite, and analyses with S content in the matrix significantly deviating from the rest of the analyses were excluded. Analyses with insufficient pyrite to generate robust regressions were also excluded on the operator's discretion. At this stage decisions on whether to use "pyrite+matrix" or "pyrite only" regressions were made, and the majority of elements were processed with the

default "pyrite+matrix" option. For elements of low abundance, "pyrite+matrix" was consistently the most robust option.

The last step involved calculating the final compositions of pyrite as well as other parameters such as uncertainties, detection limits, pyrite-free mixed compositions, and averages of the matrix which were exported to the database. An example of data reduction for a sample with an average composition of pyrite-matrix mixtures and the calculated compositions of pyrite grains are presented in Figure 8 and the average data and calculated pyrite compositions are presented as supplementary material.

Discussion

Existing algorithms for deconvolution of mineral-matrix mixtures by regression analysis

Regression analysis is routinely applied at different stages of reduction of LA-ICP-MS data, including calibration curves and modelling downhole fractionation (e. g., Paton et al. 2010). Regression is also extensively used during post-processing of data obtained by LA-ICP-MS, including estimations of compositions when proper quantification of analyses is not possible. For example, Izmer et al. (2013) used regression analysis of LA-ICP-MS data of an Archean impact spherule layer to constrain Pt/Ir ratio of the impactite. Another study has derived the compositions of ash particles by applying regression to LA-ICP-MS analyses of mixtures of ash and mineral phases (Spears 2004).

In a pioneering study, Rubatto and Hermann (2007) used regression analysis for calculation of compositions of small experimental zircon grains in a silicate glass matrix.

Mixes of zircons with glass and other minerals were analyzed by a laser beam 19-32 μm in diameter. The preliminary compositions of mixed analyzes were calculated assuming CaO content of the glass measured by EPMA. The regression equations were calculated relative to Zr and extrapolated to Zr contents in zircon measured by EPMA. A test experiment was conducted, where a mix of crushed zircon crystal of a known composition was melted with granitic melt by fast heating, which precluded reaction of melt and the mineral. The regression analyses of the mixtures reproduced the composition of the zircon starting material. In some experiments, zircons were analyzed both in the glass matrix and included in garnet; the compositions calculated by a regression for both cases produced consistent results. LA-ICP-MS analyses averaged multiple grains and zones within individual grains, producing consistent results from multiple analyses. The averages obtained matched well the averages of multiple EPMA analyses, and also had significantly smaller uncertainty compared to the EPMA data. Therefore, Rubatto and Hermann (2007) concluded that the compositions of zircons obtained from regression of LA-ICP-MS data were especially suitable for estimation of partitioning of elements between zircon and melt.

The study by Stepanov et al. (2012) applied regression analysis for calculation of the composition of monazite grains, which ranged in size from <1 μm to >1 mm, in silicate glass. The preliminary compositions of mixes of monazite and glass were calculated by using Si content in glass measured by EPMA. The regressions were calculated relative to Ce, which is the major element in monazite. The linear regression equations were calculated using all monazite and glass analyses from an experimental charge. Cerium concentration was used as the explanatory variable for calculating

379 monazite compositions. The precision of calculated compositions was estimated from
380 regression statistics and accuracy was assessed by EPMA of several REE in monazite and
381 also by a comparison of results of regression-based calculations with spot analyses of
382 larger monazite grains. The estimated errors of regressions increased with decrease of
383 grain size of monazite and abundance of elements; however, the EPMA and LA-ICP-MS
384 data showed good agreement.

385 The applications of regression analysis to deconvolution of compositions of small
386 grains of accessory minerals is not limited to LA-ICP-MS. Taylor et al. (2015) employed
387 regression analyses for calculation of compositions of small zircons crystals (<15 μm
388 long and 1-3 μm wide), which were analyzed together with glass by Secondary Ion Mass
389 Spectrometer (SIMS) with a 20-25 μm spot. Silicon content in glass measured by EPMA
390 was used as the internal standard for calculating preliminary compositions.
391 Concentrations of REEs were calculated by a regression relative to Zr contents. Another
392 approach involved calculating the amount of zircon in the ablated material using digital
393 processing of SEM images of the analyzed spots with an assumption that the amount of
394 zircon remained constant due to shallow depths of ablation pits. Comparison of zircon
395 composition obtained from regression and image analysis demonstrated a satisfactory
396 agreement though the latter showed slightly overestimated the REE concentrations.

397 New developments and future directions in deconvolution of mixed
398 LA-ICP-MS data

399 The previous studies demonstrated the utility of regression analysis for estimating
400 compositions of small grains in homogeneous matrixes by LA-ICP-MS and SIMS and
401 now this approach appears to be one of the main methods for measurement of

402 experimentally-derived partitioning coefficients between accessory minerals and melts.
403 The review of previous works summarized in Table 2 demonstrates that when regression
404 analysis is applied to the mixed LA-ICP-MS data, common issues arise such as the
405 necessity to choose which element will be used as the explanatory variable, internal
406 standards for primary quantification, and the concentration of an explanatory variable
407 used for calculating the mineral composition from the regressions.

408 This contribution further develops the regression method by applying it to
409 analysis of sulfide minerals in a complex sedimentary matrix. Sedimentary matrix in
410 black shales is different from experimental glasses by higher micro-scale heterogeneity,
411 and is thus unsuitable for analysis by EPMA. Without external EPMA data, an alternative
412 method of primary quantification based on normalization to a total was applied in this
413 work.

414 The principal differences of the new algorithm from the previous work (Rubatto
415 and Hermann 2007; Stepanov et al. 2012; Taylor et al. 2015) include: automatic
416 segmentation of the data to intervals of identical length; normalization to a total for
417 preliminary internal standardization; and calculation of the final values by choosing the
418 value of the independent variable such that the total composition of the mineral of interest
419 sums to 100%. The advantages of our algorithm include: less subjective data processing;
420 elimination of the need for EPMA data; and internal consistency of the results. An
421 additional benefit of normalization to a total is the distribution of analytical uncertainties
422 between all measured elements (Leach and Hieftje 2000). Measurement of phase
423 compositions by deconvolution of mixed data could find multiple applications to various
424 Earth science problems and data could be collected with wide diversity of

instrumentation. Recent models of mass spectrometers (e.g., triple quad and sector field ICP) provide advantages in reduction of interferences and increase of sensitivity. However, it seems that instruments with fast scan across wide range of masses and ability to record quickly changing transient signal are most suitable for the acquisition of mixed data. In this context time-of-flight (TOF) ICP-MS instruments with their ability of simultaneous measurement of multiple masses and extremally fast acquisition could be especially interesting for these applications.

This study deals with data collected in spot mode, however, LA-ICP-MS imaging/mapping is another approach for analysis of heterogeneous materials (e. g., Large et al. 2009). Segmentation of the data could be achieved from content of an element strongly concentrated in the mineral of interest or from more complicated algorithms such as the Monocle add-on in the Iolite program (Petrus et al. 2017). However, calculation of regressions, limits of detection and uncertainties from data with different numbers of contributing pixels/sweeps is more complicated and requires further development.

Sources of analytical uncertainty

The overall uncertainty of analyses arises from several sources, some of which are typical for all LA-ICP-MS analyses, whereas others are specific to the data reduction algorithm presented in this work. Regressions of different elements show characteristically different regression uncertainties (Fig. 9). The best regressions are typically observed for Ni, Co, As, Se and Sb with the estimated concentration uncertainties commonly < 10% (Fig. 9). These are elements which are most efficiently concentrated in sedimentary pyrite

(Gregory et al. 2015). Low abundance elements such as Au, Ag, Bi and Te commonly have larger uncertainties, which could be attributed to the limitations of counting statistics. The elements which commonly demonstrate poor regression relative to Fe and S include Pb, Zn, Cd and Cu and regression uncertainties could be >100 % (exceptions are also common; e.g. Figure 3 shows a perfect correlation of Pb and S in pyrite). Poor regressions might be related to the concentration of these elements in micro-inclusions of other sulfides such as galena, sphalerite and chalcopyrite within pyrite (Gregory et al. 2015; Hu et al. 2018). Despite the occurrence of these minerals as inclusions, our algorithm can estimate the composition of the compound sulfide, because we utilize S as the explanatory variable. The large uncertainties on individual measurements can be mitigated by increasing the number of pyrite analyses within a sample, which would lower the uncertainties of weighted averages and better constrain statistical distributions of elements in pyrite and matrix. Another approach could be pooling of multiple pyrite analyses for a single regression; however, in this case the data on pyrite heterogeneity will be lost.

Counting statistics is the principal source of uncertainty in the measurement of elements of low abundance. Plots of relative regression uncertainty versus concentration show negative correlations (Fig. 10). The minimum observed error increases linearly with decrease of element abundance in pyrite. Many analyses of As and Cu show substantially higher error than the minimum value defined by the counting statistics. These analyses could be explained by internal heterogeneity of these elements in pyrite. Uncertainties on Se show a good correlation with Se content suggesting homogeneous Se distribution in pyrite in agreement with observations by Large et al. (2019).

A potential source of systematic uncertainty could be different matrix-controlled fractionation in analyses rich in silicate minerals. These effects would affect the intercept of regression line. However, considering that the slope is mostly defined by the pyrite analyses, the effect of the matrix effects on pyrite composition is expected to be smaller than the fractionation.

Sulfur is a difficult element for LA-ICP-MS due to high ionization potential, interferences from dimers of oxygens and high volatility, which leads to fractionation from other elements (Gilbert et al. 2014b). Because S is used as the explanatory variable in the calculation of regressions and by the normalization to a total content of all chalcophile elements, the uncertainty in sulfur contents affects all other calculated concentrations. Individual pyrite compositions calculated by regression may show significant variations in Fe and S contents (Fig. 11), however, the agreement of the averages with the stoichiometric composition of pyrite validates the analytical approach.

In LA-ICP-MS analyses of minerals and glasses, heterogeneity of reference materials and instrumental drift are significant sources of uncertainty (e. g., Danyushevsky et al. 2011). The comparison of these values with the regression uncertainties (Table 3), however, suggests that heterogeneity of reference materials is minor relative to other uncertainties during the analysis of sedimentary pyrite.

Analysis of non-sulfidic Fe content by LA-ICP-MS in the black shales

Sedimentary rocks contain Fe in a range of minerals which could be important for understanding of geochemistry of these rocks. For example, total Fe_T content in the rock could be divided into highly reactive Fe (Fe_{HR}), which then could be subdivided to Fe in

494 pyrite (Fe_{Py}), carbonate (Fe_{carb}) and oxide (Fe_{ox}) (Canfield et al. 1986). The non-reactive
495 Fe component could be hosted by the silicate minerals (Canfield et al. 1986; Huerta-Diaz
496 and Morse 1990). Iron speciation of sedimentary rocks is one of characteristic parameters
497 used for estimating the conditions of sedimentation and digenesis and contents of
498 different Fe species could be determined by wet chemistry methods such as sequential
499 acid digestions (Canfield et al. 1986; Huerta-Diaz and Morse 1990; Liu et al. 2016).

500 Spot LA-ICP-MS analyses of pyrite-free matrix could also be used for estimating
501 *in situ* Fe contents in the sedimentary matrix. However, analyses of the matrix commonly
502 contain S and display correlations between Fe and S. These correlations suggest that
503 analyses of such matrixes also contain nano-grains of pyrite and the Fe content of these
504 analyses is higher than $Fe_{non\text{-}Py}$. Regression analysis could be used for correcting for the
505 presence of micro-grains of pyrite in the matrix analyses and calculating the true *in situ*
506 $Fe_{non\text{-}Py}$. The regression of normalized Fe versus S produces a line whose slope is
507 controlled by the ratio of Fe and S in pyrite and extrapolates to the composition of pyrite.
508 The value of the intercept of the regression line is the content of Fe at zero S content and
509 hence it represents $Fe_{non\text{-}Py}$ value. Therefore, Eq. 4 could be simplified to:

510 $$C_{Fe\ non\text{-}Py}=B_{Fe} \quad (11)$$

511 If the regression line intercept is negative, then regression might suggest that some S is
512 present in a non-sulfidic state (for example as sulfate). However, rocks with such
513 characteristics seem to be rare among black shales as they were not encountered by our
514 study.

515 The advantages of estimating the non-sulfidic Fe by LA-ICP-MS include high
516 spatial resolution in comparison with whole rock methods, and sensitivity to low

517 concentrations of $Fe_{non\text{-}Py}$. The sensitivity for low Fe concentrations might be of particular
518 interest because the wet chemistry methods are reliable at Fe_T>0.5% wt. (Clarkson et al.
519 2014), whereas the detection limit for Fe in LA-ICP-MS analysis of the matrix is
520 typically in the range 20-100 ppm. Whole rock Fe speciation could be estimated by
521 combining the *in situ* regression data with independent measurements of the abundance
522 of pyrite in the samples.
523

524 ## Advantages of analysis of pyrite in matrix by LA-ICP-MS

525

526 Several analytical methods are used for trace element analysis of small grains
527 including EPMA, SIMS and synchrotron micro-XRF. However, LA-ICP-MS has some
528 distinctive advantages:

529 • Most of the elements occurring as impurities in pyrite can be measured by LA-ICP-
530 MS over a large range of concentrations. The ability of ICP-MS to measure wide ranges
531 of concentrations makes it possible to quantify compositions of both pyrite and matrix
532 mixtures.

533 • Requirements for sample preparation are relatively modest for LA-ICP-MS. The
534 method is suitable for analysis of porous samples with a wide range of grain sizes,
535 provided that the samples are properly degassed prior to analysis.

536 • One approach used for analysis of sedimentary pyrite involved calculation of the
537 concentrations using stochiometric Fe content as the internal standard (Scott et al. 2009).
538 This treatment results in apparent presence in the analyses of various lithophile elements.
539 For example (Scott et al. 2009) observed correlations of Al and V contents in pyrite

analyzed by this method and concluded that these elements occur as silicate inclusions. The regression method allows corrections for the presence of silicate inclusions in a sensible and consistent way.

- LA-ICP-MS analyses sample larger volumes compared to EPMA and SIMS. The larger sampling volume might be an advantage in the case of sulfides and accessory minerals. Sulfides are often highly heterogeneous (Gregory et al. 2015) and analyses utilizing small sampling volumes may require large numbers of measurements to achieve representative results. Huerta-Diaz and Morse (1990) proposed that acid digestion methods for estimating pyrite trace element compositions also have an advantage of averaging significant volumes of the mineral. However, LA-ICP-MS is preferred to the bulk methods because it allows targeted analysis of various morphological and genetic types of pyrite in the sample. This ability is especially important for applications involving analysis of sedimentary pyrite with an aim of reconstructing ocean chemistry, because a rock could contain multiple generations of pyrite including recrystallized and metamorphic pyrite (Large et al. 2007; Meffre et al. 2016; Gregory et al. 2019).
- When reference materials are not available such as in the case of Hg, regression of LA-ICP-MS data still allows calculation of ratios, which could be used for sample comparison.
- Throughput is another important parameter. The RESOlution S-155 ablation cell could host 20 mounts and with 2-3 positions reserved for reference materials 17-18 sample mounts could be analyzed in a single analytical session including measurement of multiple calibration standards during the analytical run.

Summary

We describe an algorithm for quantification of LA-ICP-MS analyses of heterogeneous samples composed of small grains of pyrite in a heterogeneous matrix. The algorithm is based on linear regressions and can accommodate the effects of matrix heterogeneity without requiring external data for quantification. The method is suitable for quantification of composition of pyrite and mixtures of pyrite with other sulfide minerals in sedimentary rocks. The output of the method includes concentrations of most chalcophile elements, uncertainties of individual measurements and detection limits. Regression analysis utilizes the wealth of information recorded in the transient signal of LA-ICP-MS analyses of complex samples and represents a new step towards the comprehensive characterization of complex geological materials.

Acknowledgements

We thank Paul Olin, Elena Lounejeva-Baturina and Ivan Belousov for the assistance with the lab work. Discussions with Dan Gregory during early stages of preparation of the manuscript were very helpful for the development of our ideas. Two anonymous reviewers are thanked for useful suggestions and corrections. Paul Tomascak has done excellent editorial work which substantially improved the manuscript. Funding was provided by the Australian Research Council, Discovery Project DP 150102578.

Supplementary materials

Supplementary materials related to this manuscript can be found online.

References

Abraitis, P.K., Pattrick, R.A.D., and Vaughan, D.J. (2004) Variations in the compositional, textural and electrical properties of natural pyrite: a review. International Journal of Mineral Processing, 74, 41–59.

Canfield, D.E., Raiswell, R., Westrich, J.T., Reaves, C.M., and Berner, R.A. (1986) The use of chromium reduction in the analysis of reduced inorganic sulfur in sediments and shales. Chemical Geology, 54, 149–155.

Clarkson, M.O., Poulton, S.W., Guilbaud, R., and Wood, R.A. (2014) Assessing the utility of Fe/Al and Fe-speciation to record water column redox conditions in carbonate-rich sediments. Chemical Geology, 382, 111–122.

Danyushevsky, L., Robinson, P., Gilbert, S., Norman, M., Large, R., McGoldrick, P., and Shelley, M. (2011) Routine quantitative multi-element analysis of sulphide minerals by laser ablation ICP-MS: Standard development and consideration of matrix effects. Geochemistry: Exploration, Environment, Analysis, 11, 51–60.

Desalvo, J.S. (1971) Standard Error of Forecast in Multiple Regression: Proof of a Useful Result. The American Statistician, 25, 32–34.

Gilbert, S.E., Danyushevsky, L.V., Goemann, K., and Death, D. (2014a) Fractionation of sulphur relative to iron during laser ablation-ICP-MS analyses of sulphide minerals: implications for quantification. Journal of Analytical Atomic Spectrometry, 29, 1024–1033.

Gilbert, S.E., Danyushevsky, L.V., Rodemann, T., Shimizu, N., Gurenko, A., Meffre, S., Thomas, H., Large, R.R., and Death, D. (2014b) Optimisation of laser parameters for the analysis of sulphur isotopes in sulphide minerals by laser ablation ICP-MS. Journal of Analytical Atomic Spectrometry, 29, 1042–1051.

Goldfarb, R.J., and Groves, D.I. (2015) Orogenic gold: Common or evolving fluid and metal sources through time. Lithos, 233, 2–26.

Gregory, D., Mukherjee, I., Olson, S.L., Large, R.R., Danyushevsky, L.V., Stepanov, A.S., Avila, J.N., Cliff, J., Ireland, T.R., Raiswell, R., and others (2019) The formation mechanisms of sedimentary pyrite nodules determined by trace element and sulfur isotope microanalysis. Geochimica et Cosmochimica Acta, 259, 53–68.

Gregory, D.D., Large, R.R., Halpin, J.A., Baturina, E.L., Lyons, T.W., Wu, S., Danyushevsky, L., Sack, P.J., Chappaz, A., Maslennikov, V.V., and others (2015) Trace element content of sedimentary pyrite in black shales. Economic Geology, 110, 1389–1410.

617 Griffin, W.L., Ashley, P.M., Ryan, C.G., Sie, S.H., and Suter, G.F. (1991) Pyrite
618 geochemistry in the North Arm epithermal Ag-Au deposit, Queensland, Australia;
619 a proton-microprobe study. The Canadian Mineralogist, 29, 185–198.

620 Guillong, M., Hametner, K., Reusser, E., Wilson, S.A., and Günther, D. (2005)
621 Preliminary characterisation of new glass reference materials (GSA-1G, GSC-1G,
622 GSD-1G and GSE-1G) by laser ablation-inductively coupled plasma-mass
623 spectrometry using 193 nm, 213 nm and 266 nm wavelengths. Geostandards and
624 Geoanalytical Research, 29, 315–331.

625 Hu, S.-Y., Evans, K., Rempel, K., Guagliardo, P., Kilburn, M., Craw, D., Grice, K., and
626 Dick, J. (2018) Sequestration of Zn into mixed pyrite-zinc sulfide framboids: A
627 key to Zn cycling in the ocean? Geochimica et Cosmochimica Acta, 241, 95–107.

628 Huerta-Diaz, M.A., and Morse, J.W. (1990) A quantitative method for determination of
629 trace metal concentrations in sedimentary pyrite. Marine Chemistry, 29, 119–144.

630 Izmer, A., Goderis, S., Simonson, B.M., McDonald, I., Hassler, S.W., Claeys, P., and
631 Vanhaecke, F. (2013) Application of laser ablation-ICP-mass spectrometry for 2-
632 dimensional mapping of element distributions in a Late Archean impact spherule
633 layer. Journal of Analytical Atomic Spectrometry, 28, 1031.

634 Large, R., Thomas, H., Craw, D., Henne, A., and Henderson, S. (2012) Diagenetic pyrite
635 as a source for metals in orogenic gold deposits, Otago Schist, New Zealand. New
636 Zealand Journal of Geology and Geophysics, 55, 137–149.

637 Large, R.R., Maslennikov, V.V., Robert, F., Danyushevsky, L.V., and Chang, Z. (2007)
638 Multistage sedimentary and metamorphic origin of pyrite and gold in the Giant
639 Sukhoi log deposit, Lena Gold Province, Russia. Economic Geology, 102, 1233–
640 1267.

641 Large, R.R., Danyushevsky, L., Hollit, C., Maslennikov, V., Meffre, S., Gilbert, S., Bull,
642 S., Scott, R., Emsbo, P., Thomas, H., and others (2009) Gold and trace element
643 zonation in pyrite using a laser imaging technique: Implications for the timing of
644 gold in orogenic and carlin-style sediment-hosted deposits. Economic Geology,
645 104, 635–668.

646 Large, R.R., Halpin, J.A., Danyushevsky, L.V., Maslennikov, V.V., Bull, S.W., Long,
647 J.A., Gregory, D.D., Lounejeva, E., Lyons, T.W., Sack, P.J., and others (2014)
648 Trace element content of sedimentary pyrite as a new proxy for deep-time ocean-
649 atmosphere evolution. Earth and Planetary Science Letters, 389, 209–220.

650 Large, R.R., Halpin, J.A., Lounejeva, E., Danyushevsky, L.V., Maslennikov, V.V.,
651 Gregory, D., Sack, P.J., Haines, P.W., Long, J.A., Makoundi, C., and others
652 (2015a) Cycles of nutrient trace elements in the Phanerozoic ocean. Gondwana
653 Research, 28, 1282–1293.

Large, R.R., Gregory, D.D., Steadman, J.A., Tomkins, A.G., Lounejeva, E., Danyushevsky, L.V., Halpin, J.A., Maslennikov, V., Sack, P.J., Mukherjee, I., and others (2015b) Gold in the oceans through time. Earth and Planetary Science Letters, 428, 139–150.

Large, R.R., Mukherjee, I., Gregory, D., Steadman, J., Corkrey, R., and Danyushevsky, L.V. (2019) Atmosphere oxygen cycling through the Proterozoic and Phanerozoic. Mineralium Deposita.

Leach, A.M., and Hieftje, G.M. (2000) Methods for shot-to-shot normalization in laser ablation with an inductively coupled plasma time-of-flight mass spectrometer. Journal of Analytical Atomic Spectrometry, 15, 1121–1124.

Liu, Y., Hu, Z., Zong, K., Gao, C., Gao, S., Xu, J., and Chen, H. (2010) Reappraisement and refinement of zircon U-Pb isotope and trace element analyses by LA-ICP-MS. Chinese Science Bulletin, 55, 1535–1546.

Liu, Y., Li, C., Algeo, T.J., Fan, J., and Peng, P. (2016) Global and regional controls on marine redox changes across the Ordovician-Silurian boundary in South China. Palaeogeography, Palaeoclimatology, Palaeoecology, 463, 180–191.

Longerich, H.P., Jackson, S.E., and Günther, D. (1996) Laser ablation inductively coupled plasma mass spectrometric transient signal data acquisition and analyte concentration calculation. Journal of Analytical Atomic Spectrometry, 11, 899–904.

Meffre, S., Large, R.R., Steadman, J.A., Gregory, D.D., Stepanov, A.S., Kamenetsky, V.S., Ehrig, K., and Scott, R.J. (2016) Multi-stage enrichment processes for large gold-bearing ore deposits. Ore Geology Reviews, 76, 268–279.

Montgomery, D.C., Peck, E.A., and Vining, G.G. (2012) Introduction to Linear Regression Analysis, 680 p. John Wiley & Sons.

Paton, C., Woodhead, J.D., Hellstrom, J.C., Hergt, J.M., Greig, A., and Maas, R. (n.d.) Improved laser ablation U-Pb zircon geochronology through robust downhole fractionation correction. Geochemistry, Geophysics, Geosystems, 11.

Petrus, J.A., Chew, D.M., Leybourne, M.I., and Kamber, B.S. (2017) A new approach to laser-ablation inductively-coupled-plasma mass-spectrometry (LA-ICP-MS) using the flexible map interrogation tool 'Monocle.' Chemical Geology, 463, 76–93.

Pitcairn, I.K., Olivo, G.R., Teagle, D.A.H., and Craw, D. (2010) Sulfide evolution during prograde metamorphism of the Otago and Alpine schists, New Zealand. Canadian Mineralogist, 48, 1267–1295.

Raiswell, R., Canfield, D.E., and Berner, R.A. (1994) A comparison of iron extraction methods for the determination of degree of pyritisation and the recognition of iron-limited pyrite formation. Chemical Geology, 111, 101–110.

691 Rickard, D., Mussmann, M., and Steadman, J.A. (2017) Sedimentary Sulfides. Elements,
692 13, 117–122.

693 Rubatto, D., and Hermann, J. (2007) Experimental zircon/melt and zircon/garnet trace
694 element partitioning and implications for the geochronology of crustal rocks.
695 Chemical Geology, 241, 38–61.

696 Spears, D.A. (2004) The use of laser ablation inductively coupled plasma-mass
697 spectrometry (LA ICP-MS) for the analysis of fly ash. Fuel, 83, 1765–1770.

698 Stepanov, A.S., Hermann, J., Rubatto, D., and Rapp, R.P. (2012) Experimental study of
699 monazite/melt partitioning with implications for the REE, Th and U geochemistry
700 of crustal rocks. Chemical Geology, 300–301, 200–220.

701 Taylor, R.J.M., Harley, S.L., Hinton, R.W., Elphick, S., Clark, C., and Kelly, N.M.
702 (2015) Experimental determination of REE partition coefficients between zircon,
703 garnet and melt: a key to understanding high- *T* crustal processes. Journal of
704 Metamorphic Geology, 33, 231–248.

705 Thompson, J.M., Meffre, S., and Danyushevsky, L. (2018) Impact of air, laser pulse
706 width and fluence on U–Pb dating of zircons by LA-ICPMS. Journal of
707 Analytical Atomic Spectrometry, 33, 221–230.

708 Tomkins, A.G. (2013) On the source of orogenic gold. Geology, 41, 1255–1256.

709 Wells, J.D., and Mullens, T.E. (1973) Gold-Bearing Arsenian Pyrite Determined by
710 Microprobe Analysis, Cortez and Carlin Gold mines, Nevada. Economic Geology,
711 68, 187–201.

712 Zhou, L., McKenna, C.A., Long, D.G.F., and Kamber, B.S. (2017) LA-ICP-MS
713 elemental mapping of pyrite: An application to the Palaeoproterozoic atmosphere.
714 Precambrian Research, 297, 33–55.

715

716 Figure captions

717

718 Figure 1: Examples of textures in pyrite-bearing black shales in reflected light: a) Pyrite

719 (Py) grains of variable size disseminated in the matrix and replacing fragments; b) Partly

720 recrystallized framboidal pyrite typical for sedimentary rocks; c) Centimeter sized pyrite

721 nodule (concretion) with significant content of inclusions of sedimentary matrix in pyrite
722 and abundant inclusions of chalcopyrite (Cpy).
723
724 Figure 2: Examples of time-resolved LA-ICP-MS profiles of fine-grained pyrite in
725 silicate sedimentary matrix. a) Analysis with high pyrite content at the beginning
726 decreasing over the course of the analysis. The results of segmentation of this analysis are
727 presented in the Figure 3. b) Analysis containing both pyrite and matrix. c) Analysis of
728 relatively clean pyrite with small contribution of matrix.
729
730 Figure 3: An example of correlations between chalcophile elements and sulfur in
731 segmented pyrite and matrix analyses calculated by normalization on total. Sulfur is
732 plotted on horizontal axis and the concentrations of elements are shown on vertical axis.
733 The matrix analyses are characterized by the low S contents and lower content of
734 majority of chalcophile elements, which results in regressions with positive slopes. For
735 Zn and Cd the calculated regressions point to values lower than the estimated detection
736 limits. Fe-S regression has a positive intercept (Fe at zero S content), which suggests that
737 some of Fe in the matrix is in non-sulfide state.
738
739 Figure 4: Examples of special regression cases. Top diagrams show Fe-S plots, which
740 demonstrate mixtures of pyrite and matrix in the analyses, bottom diagrams show
741 examples of trace elements where “pyrite+matrix” and “pyrite only” regressions produce
742 different results. a) Tl content in matrix is highly heterogeneous and ‘pyrite+matrix’
743 regression predicts Tl content below the limit of detection. The regression based on

744 'pyrite only' analyses is preferred. b) Correlation of As and S suggests that As content in
745 the matrix mixed with pyrite was higher than measured. Therefore, As content in pyrite
746 was calculated by 'pyrite only' regression. c) Analyses of pyrite in a sample without
747 clean matrix but with inclusions of silicates in pyrite. Regression of segmented analyses
748 could be used for calculation of pyrite composition even when both pyrite and silicates
749 are heterogeneous, however see Figure 5 for the case of non-robust regression.
750
751 Figure 5: Negative correlation between Fe and S could result in set of non-robust
752 regression equations which are unsuitable for prediction of mineral composition. Forcing
753 the regression through the origin could solve this problem.
754
755 Figure 6: The error envelope of uncertainty on the mean. The uncertainty increases away
756 from the average of the population. The uncertainty calculated from matrix and mixed
757 pyrite-matrix analyses could overestimate the uncertainty; however, the uncertainty based
758 on mixed pyrite-matrix analyses is considered to be realistic. Here and elsewhere the
759 uncertainty is calculated for 90% confidence interval.
760
761 Figure 7: Examples of Hg in the sedimentary rocks as revealed by LA-ICP-MS of pyrite
762 bearing black shales. The vertical axis shows background corrected Hg/Fe count ratios
763 multiplied by 1000 for convenience. a) drilling through pyrite reveals significant Hg
764 content in pyrite and lower Hg/Fe ratios in the matrix. b) analysis of almost clean pyrite
765 with higher Hg/Fe ratios than sedimentary matrix. c) drilling through pyrite (with very

766 low Hg/Fe ratios) into the matrix with higher Hg/Fe ratios; the regression suggests Hg
767 below the limit of detection in this case.
768
769 Figure 8. An example of a set of pyrite analyses calculated for a sample of black shale.
770 Empty circles show the compositions of pyrite-matrix mixtures and the filled circles
771 show compositions of pyrite calculated by the regression analysis. The error bars show
772 regression uncertainties for 90% confidence intervals.
773
774 Figure 9. Relative uncertainty of the set of pyrite analyses from a sample of black shale.
775 The uncertainties are relatively low for elements strongly concentrated in pyrite.
776 However, they could reach very high values (over 100%) for such elements as Mn, Zn,
777 Cd and Tl, which are present mainly in minerals other than pyrite (Gregory et al. 2015).
778
779 Figure 10. Relative uncertainty versus concentration of an element in the analyses of
780 pyrite (all analyses were obtained with 30 μm spot size) from the data base of pyrite
781 compositions from black shales (Large et al. 2014). Good correlation of uncertainty and
782 concentration suggest Se concentration is usually homogeneous in pyrite and the
783 uncertainty is controlled by the counting statistics. For As and Cu, the correlation is much
784 weaker, suggesting that heterogeneous distribution of these elements in pyrite commonly
785 contributes to uncertainty.
786
787 Figure 11. Histograms of Fe and S contents in pyrite calculated by the regression method
788 shows distribution is close to stochiometric for both.

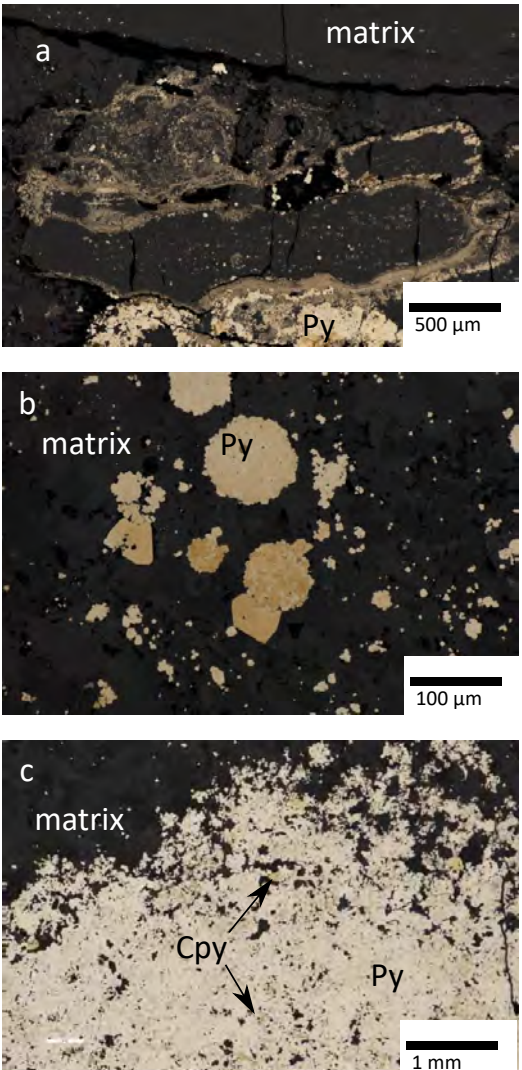

Figure 1

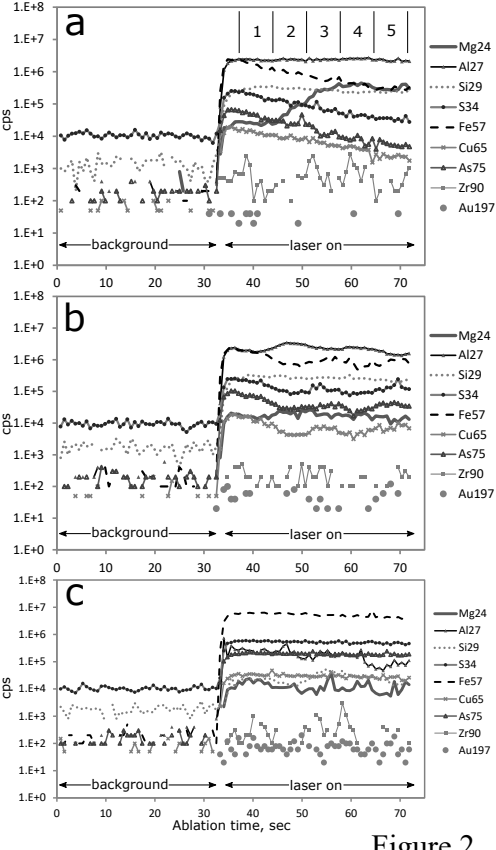
a
b
c
1
2
3
4
5
cps
1.E+8
1.E+7
1.E+6
1.E+5
1.E+4
1.E+3
1.E+2
1.E+1
1.E+0
background
laser on
0
10
20
30
40
50
60
70
Ablation time, sec
Mg24
Al27
Si29
S34
Fe57
Cu65
As75
Zr90
Au197

Figure 2

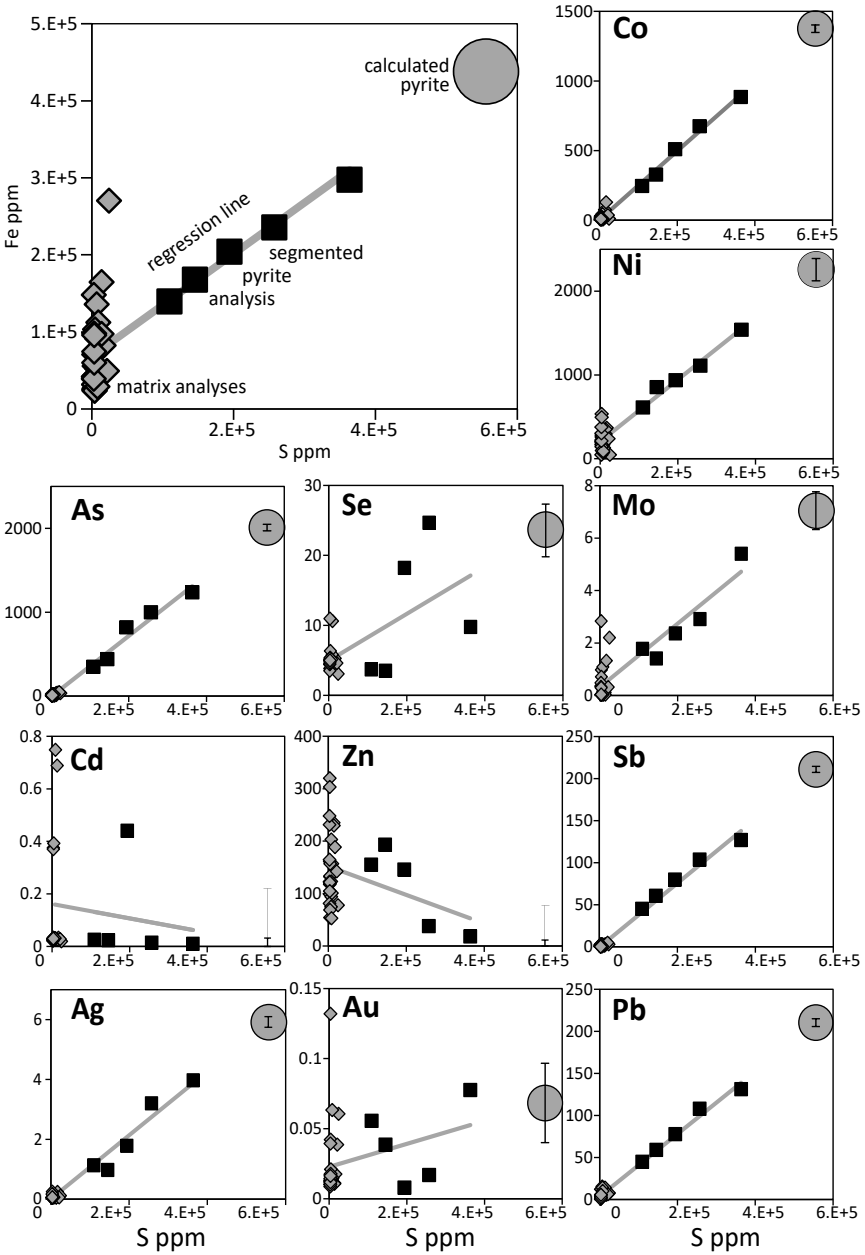
Fe ppm
S ppm
calculated pyrite
regression line
segmented pyrite analysis
matrix analyses
Co
Ni
As
Se
Mo
Cd
Zn
Sb
Ag
Au
Pb
S ppm
S ppm
S ppm

Figure 3

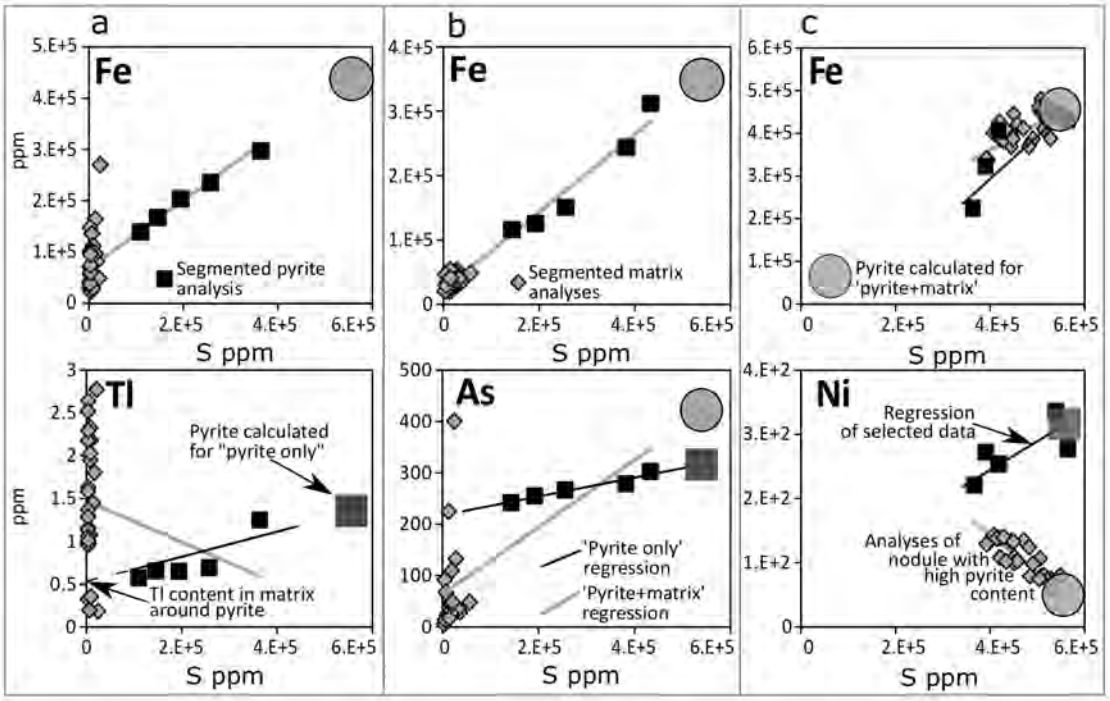
a
b
c
Fe
Fe
Fe
ppm
Segmented pyrite analysis
Segmented matrix analyses
Pyrite calculated for 'pyrite+matrix'
S ppm
S ppm
S ppm
Tl
As
Ni
Pyrite calculated for "pyrite only"
Tl content in matrix around pyrite
'Pyrite only' regression
'Pyrite+matrix' regression
Regression of selected data
Analyses of nodule with high pyrite content
ppm
S ppm
S ppm
S ppm

Figure 4

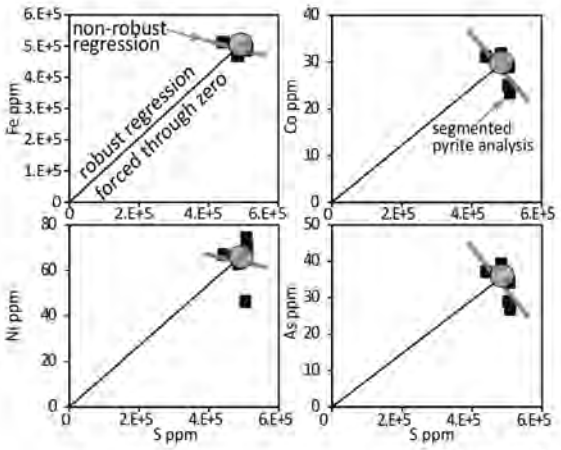
non-robust regression
robust regression forced through zero
segmented pyrite analysis
Fe ppm
Co ppm
Ni ppm
As ppm
S ppm
S ppm

Figure 5

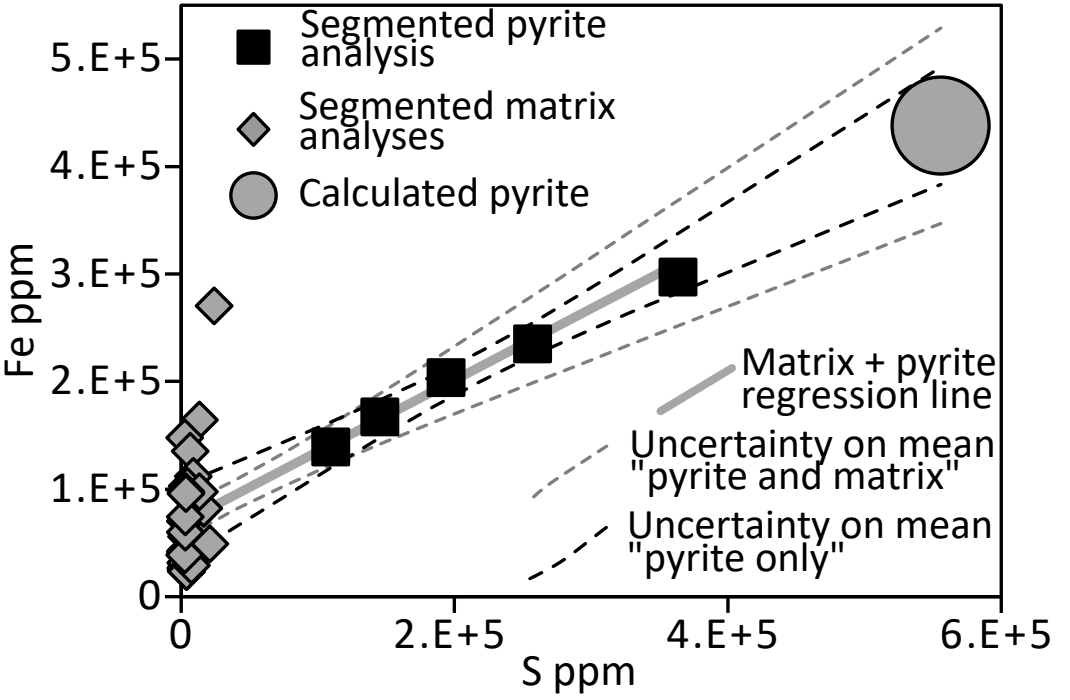
Segmented pyrite analysis
Segmented matrix analyses
Calculated pyrite
Matrix + pyrite regression line
Uncertainty on mean "pyrite and matrix"
Uncertainty on mean "pyrite only"
Fe ppm
S ppm
0
1.E+5
2.E+5
3.E+5
4.E+5
5.E+5
0
2.E+5
4.E+5
6.E+5

Figure 6

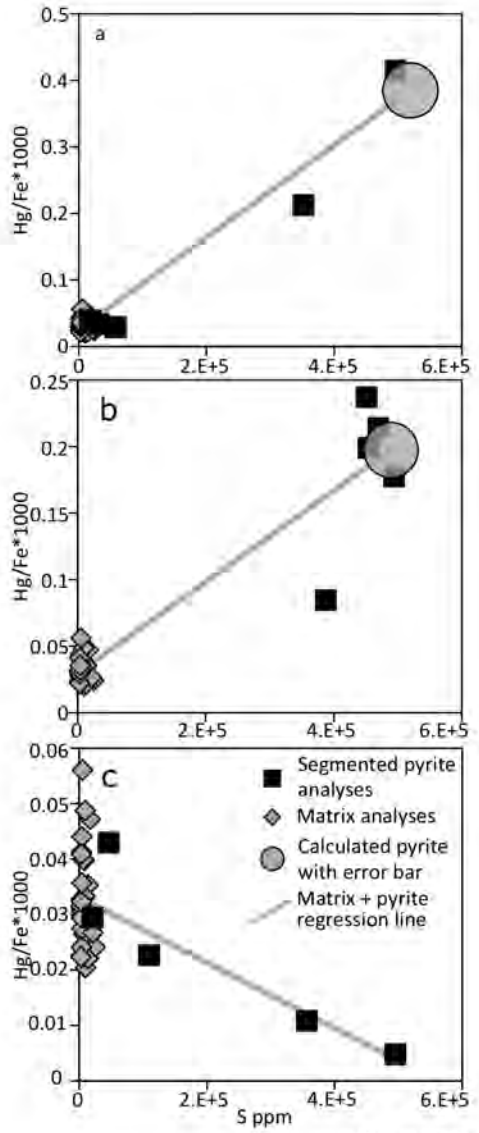
a
b
c
Hg/Fe*1000
S ppm
0
2.E+5
4.E+5
6.E+5
Segmented pyrite analyses
Matrix analyses
Calculated pyrite with error bar
Matrix + pyrite regression line

Figure 7

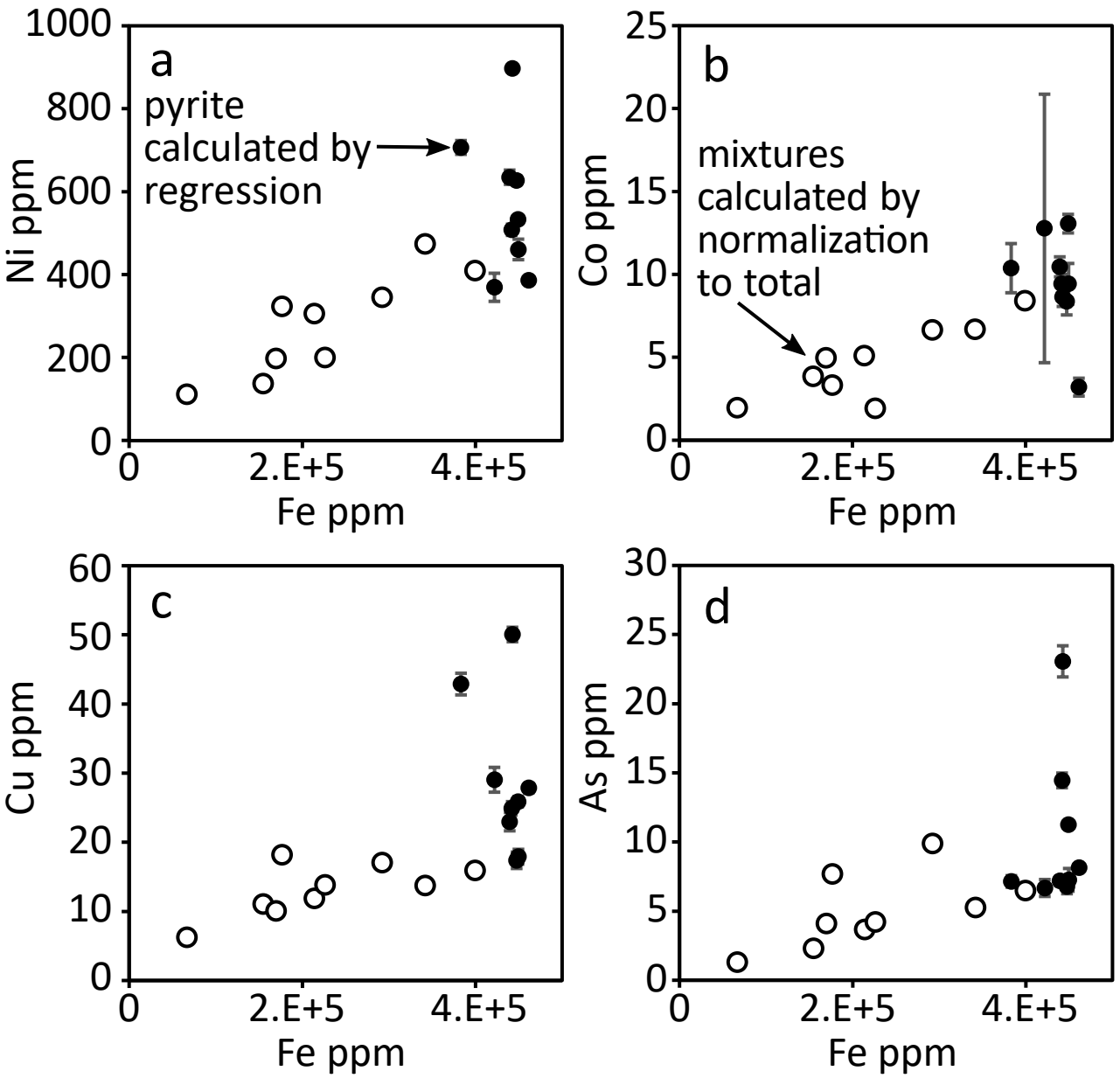
a
pyrite
calculated by
regression
Ni ppm
Fe ppm
1000
800
600
400
200
0
0
2.E+5
4.E+5
b
mixtures
calculated by
normalization
to total
Co ppm
Fe ppm
25
20
15
10
5
0
c
Cu ppm
Fe ppm
60
50
40
30
20
10
0
d
As ppm
Fe ppm
30
25
20
15
10
5
0

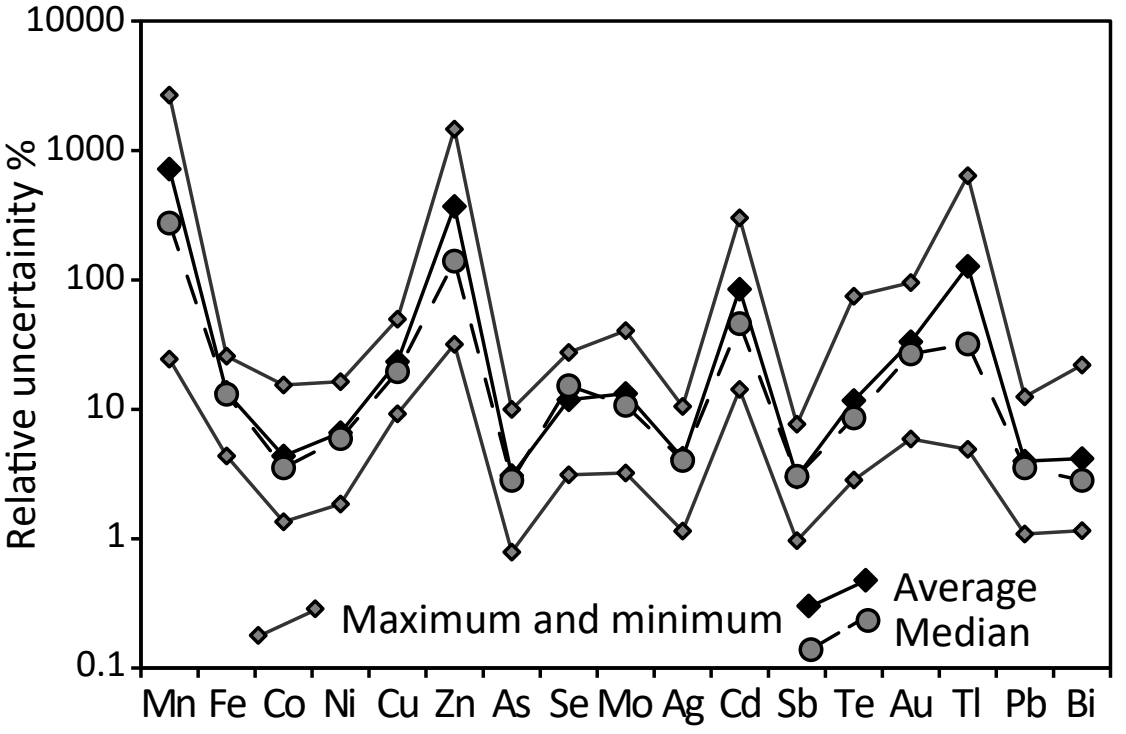
10000
1000
100
10
1
0.1
Relative uncertainity %
Mn Fe Co Ni Cu Zn As Se Mo Ag Cd Sb Te Au Tl Pb Bi
Maximum and minimum
Average
Median

Figure 9

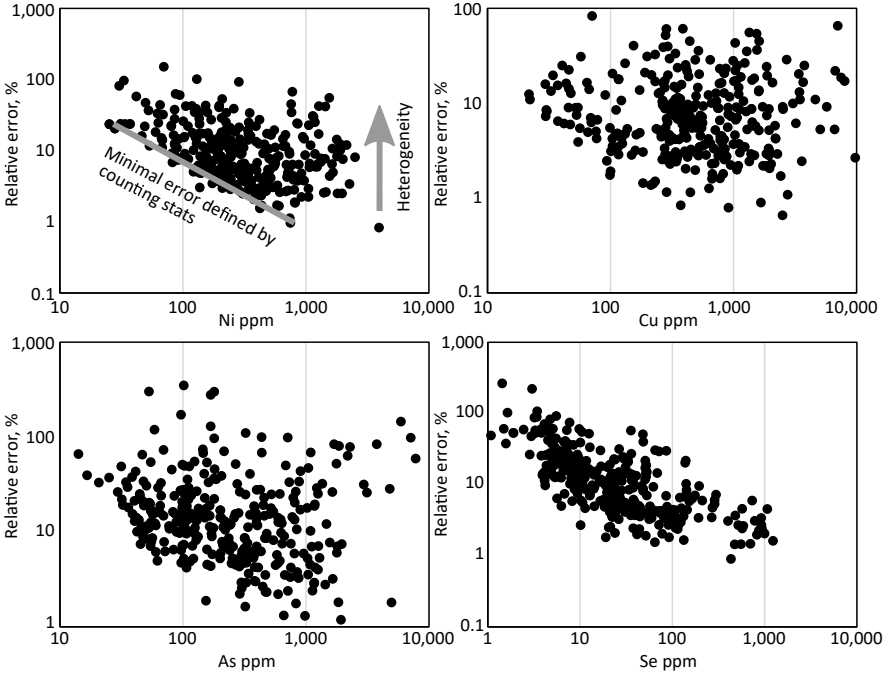
Relative error, %
1,000
100
10
1
0.1
10
100
1,000
10,000
Ni ppm
Minimal error defined by counting stats
Heterogeneity
Cu ppm
As ppm
Se ppm

Figure 10

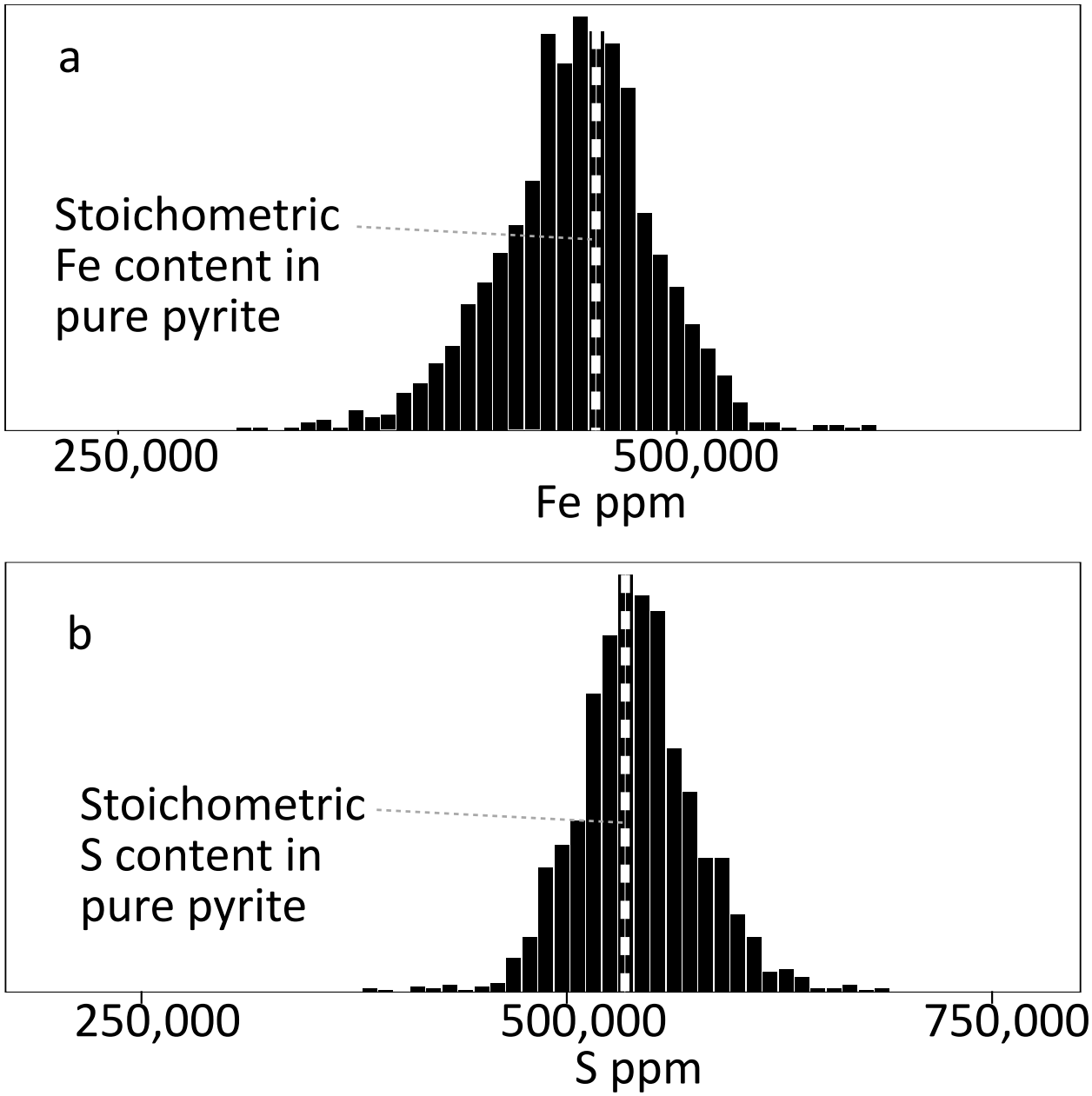
a
Stoichometric
Fe content in
pure pyrite
250,000
500,000
Fe ppm
b
Stoichometric
S content in
pure pyrite
250,000
500,000
750,000
S ppm

Figure 11

Tables

Table 1: Layout of analyzed elements, dwell times and standards used for quantification.

Elements	Dwell time	Isotope	Reference materials used for calibration	Calculated in pyrite by regression
Na	0.005	23	GSD-1G	
Mg	0.005	24	GSD-1G	
Al	0.005	27	GSD-1G	
Si	0.005	29	GSD-1G	
S	0.005	34	PPP-1	+
K	0.005	39	GSD-1G	
Ca	0.005	43	GSD-1G	
Ti	0.005	49	GSD-1G	
V	0.005	51	GSD-1G	
Cr	0.005	53	GSD-1G	
Mn	0.005	55	GSD-1G	+
Fe	0.01	57	GSD-1G	+
Co	0.04	59	STDGL2b2	+
Ni	0.02	60	STDGL2b2	+
Cu	0.02	65	STDGL2b2	+
Zn	0.02	66	STDGL2b2	+
As	0.01	75	STDGL2b2	+
Se	0.04	77	STDGL2b2	+
Rb	0.02	85	GSD-1G	
Sr	0.02	88	GSD-1G	
Zr	0.01	90	GSD-1G	
Mo	0.02	95	STDGL2b2	+

Ag	0.02	107	STDGL2b2	+
Cd	0.02	111	STDGL2b2	+
Sn	0.02	118	STDGL2b2	
Sb	0.02	121	STDGL2b2	+
Te	0.05	125	STDGL2b2	+
Ba	0.01	137	GSD-1G	
Gd	0.005	157	GSD-1G	
Hf	0.01	178	GSD-1G	
Ta	0.01	181	GSD-1G	
W	0.02	182	STDGL2b2	
Pt	0.05	195	STDGL2b2	+
Au	0.05	197	STDGL2b2	+
Hg	0.02	202		
Tl	0.02	205	STDGL2b2	+
Pb	0.02	206	STDGL2b2	+
Pb	0.02	207	STDGL2b2	+
Pb	0.02	208	STDGL2b2	+
Bi	0.02	209	STDGL2b2	+
Th	0.01	232	GSD-1G	
U	0.01	238	GSD-1G	

Table 2: Summary of principal parameters used in different studies which applied regression analysis to the deconvolution of mixed LA-ICP-MS data.

	Mineral of interest	Matrix	Method	Internal standard or primary quantification	Explanatory (independent) variable	Explanatory variable value for regression	Data used to constrain regression
Rubatto and Hermann (2007)	Zircon	Glass and garnet	LA-ICP-MS	Ca	Zr	EPMA	Mineral plus matrix
Stepanov et al. (2012)	Monazite	Glass	LA-ICP-MS	Si	Ce	EPMA	Mineral plus matrix
Taylor et al. (2015)	Zircon	Glass	SIMS	Si	Zr	EPMA	Mineral plus matrix
Present study	Pyrite	Sediment	LA-ICP-MS	Fe for preliminary quantification; followed by normalisation to 100%	S	Calculated from set of regressions with 100% total requirement.	Two options: 'pyrite+ matrix' and 'pyrite only'

Table 3: Sources of uncertainty of the data on the example of set of pyrite analyses.

Elements	Standard uncertainty %	Drift	Drift Error %	Average error %	Maximum error %	Minimum error %
				Regression errors		
Na	0.2	0.97	0.4			
Mg	0.04	0.98	0.6			
Al	0.3	0.97	0.7			
Si	0.8	0.94	1.2			
S			10.0			
K	0.1	0.98	0.6			
Ca	0.1	0.98	2.7			
Ti	0.06	1.01	1.1			
V	2	1.01	1.5			
Cr	3	1.06	3.8			
Mn	20	1.00	1.7	717	2672	24
Fe	0.1			13	26	4
Co	2	0.97	1.5	4	15	1
Ni	4	0.99	1.1	7	16	2
Cu	2	0.96	1.9	23	50	9
Zn	2	1.00	0.8	368	1465	32
As	8	1.05	1.4	3	10	1
Se	1	0.64	1.8	12	27	3
Rb	0.4	1.06	2.7			
Sr	0.7	1.08	0.5			
Zr	2	1.02	0.9			
Mo	3	1.10	4.4	13	40	3
Ag	3	1.02	4.2	4	11	1
Cd	4	1.05	1.9	84	301	14
Sn	6	1.07	1.9			
Sb	7	1.04	1.3	3	8	1

Te		0.89	0.3	12	75	3
Ba	1	1.06	2.3			
Gd	0.5	1.28	3.5			
Hf	2	1.14	1.4			
Ta	4	1.10	0.6			
W	4	1.17	2.1			
Pt		0.77	43.7			
Au		0.82	14.7	33	95	6
Hg						
Tl	0.1	0.70	11.7	127	636	5
Pb	2	1.11	1.3	4	12	1
Bi	4	1.06	1.5	4	22	1
Th	2	1.06	2.8			
U	2	1.09	2.4			